

Natural Balance of Multicell Converters

R.H. Wilkinson and H. du T. Mouton
 Power Electronics Group
 Dept. of Electrical and Electronic Engineering
 University of Stellenbosch
 Private Bag X1
 Matieland, 7602
 South Africa
 Telephone: +27-(0)21-808-4455
 Fax: +21-(0)21-808-4981
 E-mail: rwilknsn@sun.ac.za, dtmouton@sun.ac.za

T.A. Meynard
 Laboratoire d'Electrotechnique et d'Electronique Industrielle
 ENSEEIHT, Institut National Polytechnique de Toulouse
 Unité Mixte de Recherche du CNRS N° 5828
 2, rue Camichel, B.P.7122
 31071 Toulouse, Cedex 07
 France
 Telephone: +33-(0)5-61-58-83-58
 Fax: +33-(0)5-61-62-49-69
 E-mail: meynard@leei.enseeiht.fr

Abstract—The multicell converter topology is said to possess a natural voltage balancing property. This paper models multicell converters for the general case of p -cells. It describes the relationship between the models for different numbers of cells in a generic model for a p -cell multicell converter. The switching functions used in switching these converters are mathematically analyzed. Equivalent circuits are derived and presented. The switching and balancing properties of these converters are mathematically analyzed. Multicell converters were modeled previously for both sinusoidal and fixed duty-cycle references. The model discussed in this paper is valid for any modulation method. The conditions for balanced cell capacitor voltages are presented from the aforementioned mathematical synthesis. The balancing property of these converters is also proved mathematically from the presented properties and conditions for natural balancing are discussed. The balancing properties and conditions are formulated and presented as a “Natural Balance Theory for Multicell Converters”. Simulation and experimental results are included to verify the presented balance theory and properties. Conclusions presented include conditions for the theory to be valid as well as possible extensions to the theory and practical implications on converter design.

I. INTRODUCTION

Multilevel converters were developed as a result of a growing need for higher power converters. In order to achieve this higher power rating, the voltage and current capabilities of the devices used in the converter need to be increased. Current IGBT technology extends up to 4.5 kV 900 A per switching device [13]. Converters that make use of a series connection of switches, allow for the use of switches with reduced voltage ratings. These lower voltage switches have lower conduction losses and can switch at a higher frequency [1]. Higher switching frequencies and a smaller “voltage step” capability results in higher quality switching waveforms. This paper focuses more specifically on the natural balancing property [8],[9] of the multicell converter topology, also known as the flying capacitor multilevel converter topology. The theory discussed in this paper is different from existing balancing theories [7] in that it can be used for any modulation method.

II. THE MULTICELL TOPOLOGY

In the multicell topology, commutation cells with voltage ratings of $\frac{V_t}{p}$ are imprecated (overlapped) to form a chopper circuit or inverter leg capable of switching the voltage V_t . A diagram showing the general circuit of the multicell topology is shown in Fig. 2. The number of cells can be extended to p cells, depending on the blocking voltage needed. Control signals of the different cells can be interleaved to optimize the output voltage waveform [4]. The output voltage has steps of an amplitude of $\frac{V_t}{p}$ and a frequency that is p times the switching frequency. This roughly reduces the output filter inductor by p^2 [4]. This topology can be applied to choppers

(buck-, boost-, buck-boost, Čuk-, etc.), voltage-source inverters (half-bridge, full-bridge, three-phase, etc.), current-source inverters, cycloconverters, etc. Examples of applications listed by Meynard [4] are as follows: a 1.5 kV, 3-cell 4-level sinusoidal rectifier; a 4 kV 300 A, 7-cell 8-level inverter leg switching at 3 kHz, i.e. an output voltage ripple frequency of 21 kHz; an Active Current Filter at 20 kV.

III. MATHEMATICAL MODEL

There are three different mathematical models available to represent a multicell converter. These models are as follows [1], [2]:

- **Direct or instantaneous model:** this model accurately represents the state of each cell during a switching period. All the harmonic phenomena will be present in this model.
- **Average model:** this model is obtained by replacing each switching element with its average value over a switching period T_s .
- **Harmonic model:** this model will not be discussed here. This model can be used to obtain a dynamic representation of a multicell converter by taking its harmonic phenomena into account. A detailed discussion of this model can be found in [3].

A. Two-port Switching Circuits

The concept of a two-port switching circuit [5] will be applied throughout the mathematical analysis of the multicell converter topology.

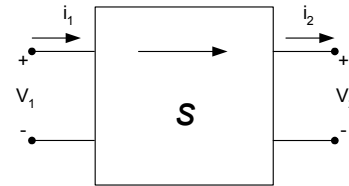


Fig. 1. Basic 2-port switching circuit.

The basic 2-port switching circuit is shown in Fig. 1. This switching circuit is controlled by a switching function $s(t)$. The arrow is pointed from port 1 to port 2. The relationship between the voltages v_1 and v_2 and the currents i_1 and i_2 are as follows:

$$v_2 = sv_1 \quad (1)$$

$$i_1 = si_2 \quad (2)$$

The switching function s can assume any real value. In the case of a multicell converter, s is the switching state of a cell and assumes the values -1 and 1.

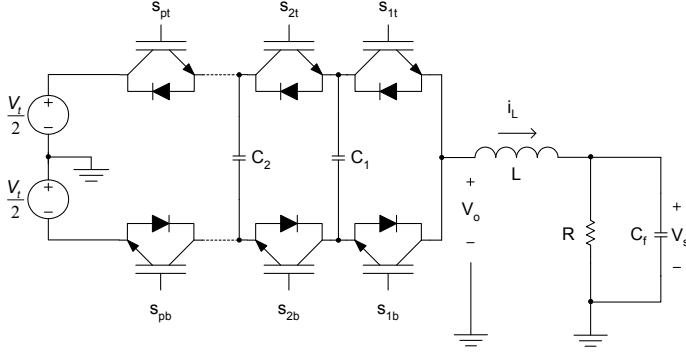


Fig. 2. A p -cell Multicell inverter.

B. Circuit Analysis

The purpose of this derivation is to obtain an instantaneous model of a multicell converter, as shown in Fig. 2, in order to ensure equal cell capacitor voltages. The following assumptions were taken into account for the instantaneous model [1]:

- Ideal switches were used; implying that the on-state voltage, off-state current, dead-times, delays and switching times were zero.

To study the balancing properties of the circuit, the following variables are defined:

- Switching functions for the cells, which can be defined as follows:

$$s_\eta(t) = \begin{cases} 1 & \text{if } S_{\eta t} \text{ is closed} \\ -1 & \text{if } S_{\eta b} \text{ is closed,} \end{cases} \text{ for } \eta = 1, \dots, p \quad (3)$$

- Difference voltage V_{d_η} which can be written as follows:

$$V_{d_\eta} = \frac{\eta V_t}{p} - V_{C_\eta} \text{ for } \eta = 1, \dots, p-1 \quad (4)$$

- Difference switching functions $s_{d_\eta}(t)$ which can be written as follows:

$$s_{d_\eta}(t) = \frac{1}{2} \{s_{\eta+1}(t) - s_\eta(t)\} \text{ for } \eta = 1, \dots, p-1 \quad (5)$$

- Total switching function $s_t(t)$ which can be written as follows:

$$s_t(t) = \frac{1}{2} \sum_{\eta=1}^p s_\eta(t) \quad (6)$$

After defining (4)-(6), the circuit differential equations can be rewritten in terms of d and t parameters as follows:

$$\frac{dV_{d_\eta}}{dt} = -\frac{1}{C_\eta} s_{d_\eta}(t) \cdot i_L(t) \text{ for } \eta = 1, \dots, p-1 \quad (7)$$

$$\frac{di_L}{dt} = \frac{1}{L} \cdot \left\{ \frac{V_t}{p} s_t(t) + \sum_{\eta=1}^{p-1} V_{d_\eta} s_{d_\eta}(t) - V_s \right\} \quad (8)$$

$$\frac{dV_s}{dt} = \frac{1}{C_f} \cdot \left(i_L(t) - \frac{V_s}{R} \right) \quad (9)$$

Based on these equations it is possible to derive an equivalent circuit in terms of d and t parameters, as discussed in [5], [6] and [10]. This circuit is shown in Fig. 3.

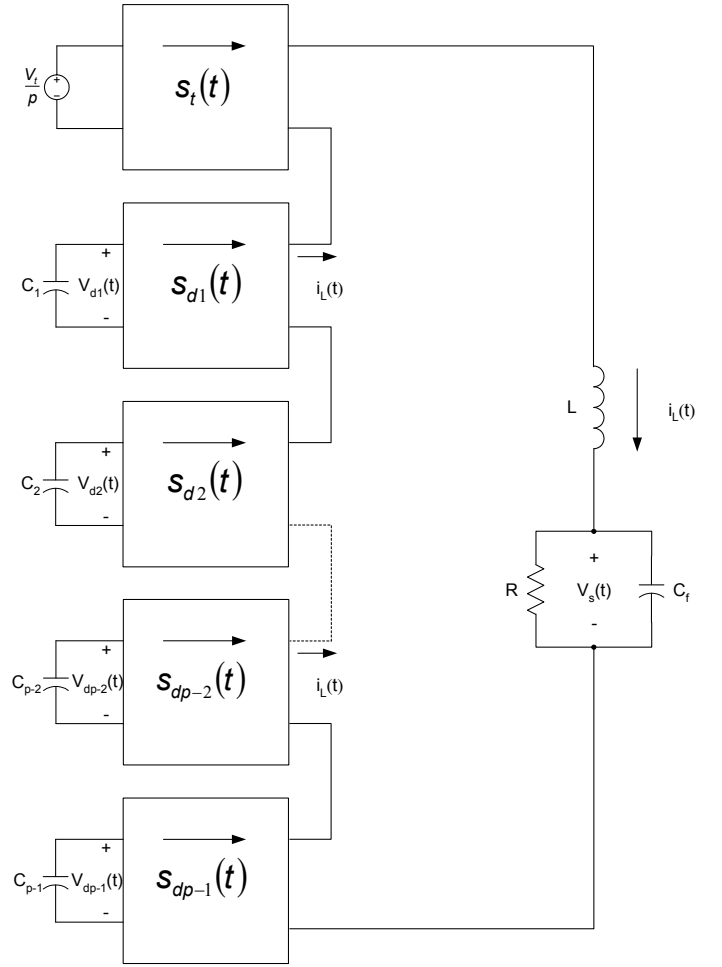


Fig. 3. Equivalent switching circuits.

C. Steady-state Analysis

In the frequency domain, the expression for the inductor current $I_L(\omega)$ can be written as follows:

$$I_L(\omega) = \frac{V_0(\omega)}{Z(\omega)} = \frac{\frac{V_t}{p} \cdot S_t(\omega)}{Z(\omega)} + \frac{\sum_{\eta=1}^{p-1} V_{d_\eta} S_{d_\eta}(\omega)}{Z(\omega)} \quad (10)$$

where $V_0(\omega)$ is the unfiltered output voltage and $Z(\omega)$ is the load impedance.

The expressions for the cell capacitor currents $I_{C_\eta}(\omega)$ can then be found by using convolution and applying the 2-port properties of the equivalent circuit in terms of d and t parameters, as shown in Fig. 3:

$$\begin{aligned} I_{C_\eta}(\omega) &= -I_L(\omega) \star S_{d_\eta}(\omega) \text{ for } \eta = 1, \dots, p-1 \\ &= -\left(\frac{\frac{V_t}{p} \cdot S_t(\omega)}{Z(\omega)} + \frac{\sum_{\eta=1}^{p-1} V_{d_\eta} S_{d_\eta}(\omega)}{Z(\omega)} \right) \star S_{d_\eta}(\omega) \end{aligned} \quad (11)$$

(Note that \star denotes convolution in the frequency domain.)

When the above equations are solved for the steady-state case of $I_{C_\eta}(\omega)|_{\omega=0} = 0$, equations that describe the unbalance of the capacitor voltages for all $p-1$ cell capacitors can be obtained. In the analysis discussed here, $\overline{S_{d_\eta}(\xi)}$ represents the complex conjugate of $S_{d_\eta}(\xi)$. Therefore, knowing that the switching functions are real valued functions, the following is true:

$$\overline{S_{d_\eta}(\xi)} = S_{d_\eta}(-\xi) \text{ for } \eta = 1, \dots, p-1. \quad (12)$$

When using PWM, the harmonics appear in groups around integer multiples (denoted by m) of the switching frequency. For sinusoidal modulation, side bands appear at integer multiples (denoted by n) of the reference frequency around these harmonics of the switching frequency. In the following mathematical analysis: the definition of convolution is applied and m is used as the number of the group of harmonics over which an integral is taken, where the group includes the side band harmonics. For convenience, the following variables are defined: λ_η , where $\eta = 1, 2, \dots, p-1$ and $k = 0, 1, \dots, \infty$:

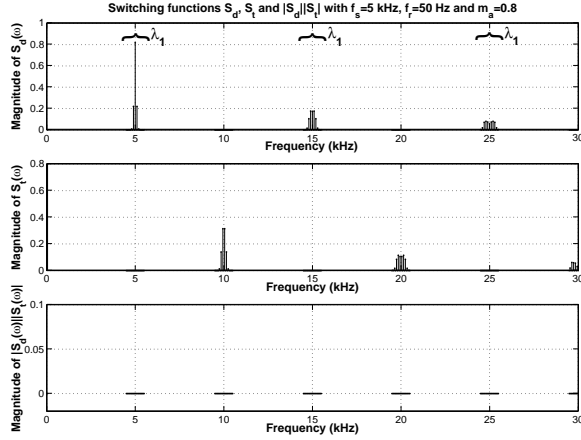
$$\lambda_\eta = \int_{m=pk+\eta} \frac{|S_{d_\eta}(\xi)|^2}{Z(\xi)} d\xi \quad (13)$$

and α_η , where $\eta = 1, 2, \dots, p-1$ and $k = 0, 1, \dots, \infty$:

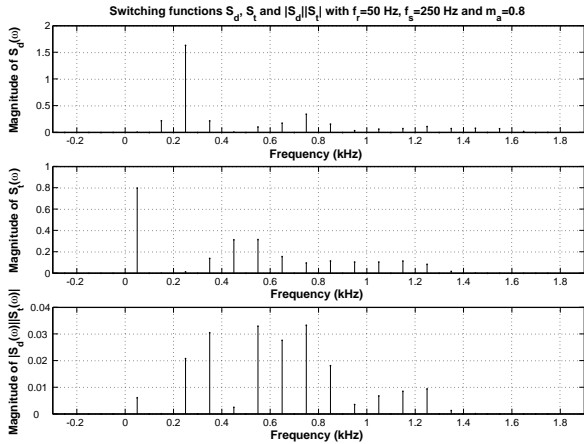
$$\alpha_\eta = \int_{m=pk+\eta} \frac{S_t(\xi) \overline{S_{d_\eta}(\xi)}}{Z(\xi)} d\xi \quad (14)$$

For the 2-cell case, using the above notation for λ_1 means that it is the integral over the frequency groups denoted by $m = 2k + 1$, for $k = 0, 1, \dots$, i.e. $m = 1, 3, \dots$ where m is a multiple of the switching frequency (see Fig. 4(a)). Using the above definitions for λ_η , it is possible to write the unbalance equations for all $p-1$ cell capacitors as follows:

$$\frac{\mathbf{V}_d}{V_t} = -\frac{1}{p} \mathbf{\Lambda}^{-1} \mathbf{A} \quad (15)$$



(a) Voltage balance.



(b) Voltage unbalance.

Fig. 4. Harmonics of interleaved modulation for a 2-cell converter.

where \mathbf{V}_d , $\mathbf{\Lambda}$ and \mathbf{A} are defined in (24).

The relationship between V_{d_η} and V_t as represented in (15) represents the relationship of the unbalance of the η^{th} cell capacitor relative to the input voltage.

For the special case of 2 cells the harmonics of S_{d_1} and S_t is shown in Fig. 4(a) and 4(b). From (15), the relationship between V_{d_1} and V_t , or the relationship of the unbalance of the cell capacitor voltage relative to the input voltage can be written as follows:

$$\begin{aligned} \frac{V_{d_1}}{V_t} &= -\frac{1}{2} \lambda_1^{-1} \alpha_1 \\ &= -\frac{1}{2} \frac{\int_{m=2k+1} \frac{S_t(\xi) \overline{S_{d_1}(\xi)}}{Z(\xi)} d\xi}{\int_{m=2k+1} \frac{|S_{d_1}(\xi)|^2}{Z(\xi)} d\xi} \end{aligned} \quad (16)$$

The effect of the harmonics on the natural balance will be discussed in Section IV paragraph D.

IV. HARMONIC ANALYSIS

A. Interleaved Switching

It was shown in [3] that for natural balance to occur, it is necessary for the duty-cycles of the respective cells to be equal and for the phase-shift of each successive control signal to be equal to $\frac{2\pi}{p}$. For the case discussed in this paper, p triangular carrier signals phase-shifted by $\frac{2\pi}{p}$ radians were used to generate interleaved switching patterns to generate the PWM signals. Using Fourier methods developed by Bennet [11] and Black [12], it is possible to write Fourier series expansions for $s_1(t)$ to $s_p(t)$ using (25) and (26). In the above-mentioned expressions for $s_1(t)$ and $s_\eta(t)$ it is important to look at the characteristics of the Fourier coefficients. For sinusoidal modulation with a modulation index (m_a) of A , these Fourier coefficients can be written as follows:

- $m \neq 0$ and n odd:

$$A_{mn} + jB_{mn} = \frac{2j}{m\pi} J_n \left(\frac{m\pi A}{2} \right) \left(1 + e^{-jm\pi} \right) \quad (17)$$

- $m \neq 0$ and n even:

$$A_{mn} + jB_{mn} = \frac{2}{jm\pi} J_n \left(\frac{m\pi A}{2} \right) \left(1 - e^{-jm\pi} \right) \quad (18)$$

- $m = 0$ and $n = 1$:

$$A_{01} + jB_{01} = jA \quad (19)$$

- $m = 0$ and $n \neq 1$:

$$A_{0n} + jB_{0n} = 0 \quad (20)$$

The characteristics of the above coefficients can be summarized as follows:

- A_{00} : this coefficient is the dc-component of s which is zero.
- $A_{0n} + jB_{0n}$: these coefficients are the Fourier series coefficients of the reference signal.
- $A_{m0} + jB_{m0}$: these coefficients are components at the switching frequency ω_s and integer multiples thereof.
- $A_{mn} + jB_{mn}$: these coefficients are harmonic side bands around integer multiples of the switching frequency.

B. Fixed Duty-cycle Switching

For a fixed duty-cycle with a value D , where $0 \leq D \leq 1$ these Fourier coefficients can be written as follows:

- $m \neq 0$:

$$A_{m0} + jB_{m0} = \frac{4(-j)^m}{m\pi} \sin(m\pi D) \quad (21)$$

- $m = 0$:

$$A_{00} + jB_{00} = 2(2D - 1) \quad (22)$$

$$\mathbf{\Lambda} = \begin{bmatrix} \sum_{\eta=1}^{p-1} \lambda_{\eta} & \sum_{\eta=1}^{p-1} e^{j \frac{2\pi\eta}{p}} \lambda_{\eta} & \cdots & \sum_{\eta=1}^{p-1} e^{j \frac{2\pi\eta(p-2)}{p}} \lambda_{\eta} \\ \sum_{\eta=1}^{p-1} e^{j \frac{-2\pi\eta}{p}} \lambda_{\eta} & \sum_{\eta=1}^{p-1} \lambda_{\eta} & \cdots & \sum_{\eta=1}^{p-1} e^{j \frac{2\pi\eta(p-3)}{p}} \lambda_{\eta} \\ \vdots & \vdots & \ddots & \vdots \\ \sum_{\eta=1}^{p-1} e^{j \frac{-2\pi\eta(p-2)}{p}} \lambda_{\eta} & \sum_{\eta=1}^{p-1} e^{j \frac{2\pi\eta(p-3)}{p}} \lambda_{\eta} & \cdots & \sum_{\eta=1}^{p-1} \lambda_{\eta} \end{bmatrix} \quad (23)$$

$$\mathbf{A} = \begin{bmatrix} \alpha_1 \\ \alpha_2 \\ \vdots \\ \alpha_{p-1} \end{bmatrix} \quad \frac{\mathbf{V}_d}{V_t} = \begin{bmatrix} \frac{V_{d1}}{V_t} \\ \frac{V_{d2}}{V_t} \\ \vdots \\ \frac{V_{d_{p-1}}}{V_t} \end{bmatrix} \quad \mathbf{V}_d = \begin{bmatrix} V_{d1} \\ V_{d2} \\ \vdots \\ V_{d_{p-1}} \end{bmatrix} \quad \mathbf{V}_{d0} = \begin{bmatrix} V_{d01} \\ V_{d02} \\ \vdots \\ V_{d0(p-1)} \end{bmatrix} \quad (24)$$

$$s_1(t) = \frac{1}{2}A_{00} + \sum_{n=1}^{\infty} \{A_{0n} \cos(n\omega_r t) + B_{0n} \sin(n\omega_r t)\} + \sum_{m=1}^{\infty} \{A_{m0} \cos(m\omega_s t) + B_{m0} \sin(m\omega_s t)\} + \sum_{m=1}^{\infty} \sum_{n=\pm 1}^{\pm \infty} \{A_{mn} \cos(m\omega_s t + n\omega_r t) + B_{mn} \sin(m\omega_s t + n\omega_r t)\} \quad (25)$$

$$s_{\eta}(t) = \frac{1}{2}A_{00} + \sum_{n=1}^{\infty} \{A_{0n} \cos(n\omega_r t) + B_{0n} \sin(n\omega_r t)\} + \sum_{m=1}^{\infty} \left\{ A_{m0} \cos\left(m\omega_s t - \frac{2^{\eta-1}m\pi}{p}\right) + B_{m0} \sin\left(m\omega_s t - \frac{2^{\eta-1}m\pi}{p}\right) \right\} + \sum_{m=1}^{\infty} \sum_{n=\pm 1}^{\pm \infty} \left\{ A_{mn} \cos\left(m\omega_s t + n\omega_r t - \frac{2^{\eta-1}m\pi}{p}\right) + B_{mn} \sin\left(m\omega_s t + n\omega_r t - \frac{2^{\eta-1}m\pi}{p}\right) \right\} \quad (26)$$

C. The Effect of the Duty-cycle on the Harmonics

The Fourier coefficients of the switching functions $s_{\eta}(t)$ where $\eta = 1, \dots, p-1$ for the fixed duty-cycle case were shown in (21) and (22).

If the switching functions derived in Section IV, paragraph A are substituted into (5) the following expression results:

$$s_{d_{\eta}}(t) = - \sum_{\substack{m=pk+1, \dots, p-1 \\ k=0,1, \dots}}^{\infty} (A_{m0} \cos(m\omega_s t) + B_{m0} \sin(m\omega_s t)) \quad (27)$$

In order to find out what the effect of the duty-cycle is on the harmonics of the switching functions, it is important to note the following:

$$\frac{\sin(m\pi D)}{m\pi} = 0 \quad (28)$$

if and only if $m\pi = \kappa\pi$, where both κ and mD are integers. This means that the duty-cycle D can be written as the following fraction:

$$D = \frac{\kappa}{m} \quad (29)$$

Equation (29) implies that when κ is a factor of m , the harmonics will be zero.

D. Influence of Harmonics on Natural Balance

For the 2-cell case it was found that the harmonics of S_{d_1} were centered around odd multiples of the switching frequency ω_s and that the harmonics of S_t were centered around even multiples of the switching frequency ω_s . An example of the harmonics of interleaved switching of a 2-cell multicell inverter with a balanced cell capacitor voltage is shown in Fig. 4(a). The following equation holds for this case in steady-state:

$$|S_{d_1}(\omega)||S_t(\omega)| \approx 0 \quad (30)$$

Three cases were found in which $|S_{d_1}(\omega)||S_t(\omega)| > 0$, causing unbalance of the cell capacitor voltage:

- when the switching frequency (ω_s) is higher than the frequency of the reference signal (ω_r), but not high enough to avoid aliasing of the side-bands of the harmonic multiples thereof.
- when the reference signal contains high frequency components.
- when a fixed duty-cycle is used and the number of cells is not prime, there are certain values of the duty-cycle which can result in unbalance.

The harmonics for an unbalanced cell capacitor voltage is shown in Fig. 4(b), where it is clear that the following equation holds:

$$|S_{d_1}(\omega)||S_t(\omega)| > 0 \quad (31)$$

The principle shown in (30) can be used to simplify (15) further for the general case of p -cells.

The unbalance equations (15) can also be used to calculate the rebalancing time constant in a multicell converter. The system of differential equations describing the cell capacitor voltages is as follows:

$$\frac{d\mathbf{V}_d}{dt} = \mathbf{\Lambda} \mathbf{V}_d \quad (32)$$

This information can be used to improve the rebalancing times of the cell capacitor voltages. The general equation for the rebalancing time constants can be calculated from the system of differential equations as follows:

$$\mathbf{V}_d = e^{-\frac{2}{C} \text{Re}\{\mathbf{\Lambda}\}t} \mathbf{V}_{d0} \quad (33)$$

E. Balance Booster Circuit

In (16) it can be seen that the load impedance $Z(\omega)$ affects the natural balance. If (30) holds, the denominator of (16) can be increased by decreasing $Z(\omega)$ which will improve the balancing time. It is also important to note that $Z(\omega)$ should always contain resistance

TABLE I
SIMULATION AND EXPERIMENTAL PARAMETERS

DC-bus voltage	V_t	100 V
Switching frequency	f_s	5 kHz
Reference frequency	f_r	50 Hz
Cell capacitance	C_1, C_2	40 μF
Filter inductance	L_f	200 μH
Filter capacitance	C_f	50 μF
Load resistance	R_f	10 Ω
Balance booster inductance	L_b	237 μH
Balance booster capacitance	C_b	4.3 μF
Balance booster resistance	R_b	2.2 Ω

for the unbalance to tend to zero. If $Z(\omega)$ is purely imaginary, the average values of the unbalance may be zero, but it may be oscillating.

A balance booster circuit [3], [9] is a notch filter which is connected in parallel with the load. The purpose of this filter is to provide a low impedance at the switching frequency. For this case, a series $R_b - L_b - C_b$ circuit was used.

The reason for the name ‘‘balance booster’’, follows from the effect that this circuit has on the cell capacitor balance. If this circuit is designed to have a low impedance at the switching frequency, it means that the load impedance, $Z(\omega)$, is then smaller at the switching frequency due to the parallel combination of the load impedance and the booster circuit impedance. As an example, the value of the bottom integral in (16) increases. This effect is shown in section V through simulation and theoretical results.

V. SIMULATIONS AND THEORETICAL RESULTS

Multicell inverters, using the topology as shown in Fig. 2 with $p = 2$ and $p = 3$, were simulated using Simplorer®. The simulations were performed with the parameter values as listed in Table I. The theory discussed in this paper was implemented in Matlab®. The results obtained in the simulations are compared with the theoretical results for both sinusoidal and fixed duty-cycle modulation. The initial voltages of the cell capacitors were zero for all the cases. Fig. 5(a), 6(a) and 7(a) show the cell voltage unbalance decay for a 2-cell converter with different modulation indices without a balance booster connected across the load, while Fig. 5(b), 6(b) and 7(b) show the case when a balance booster is used. The same approach was used for a 3-cell case and the results are shown in Fig. 8 to 10. Fig. 11 and 12 show the fixed duty-cycle results. The balance booster circuit

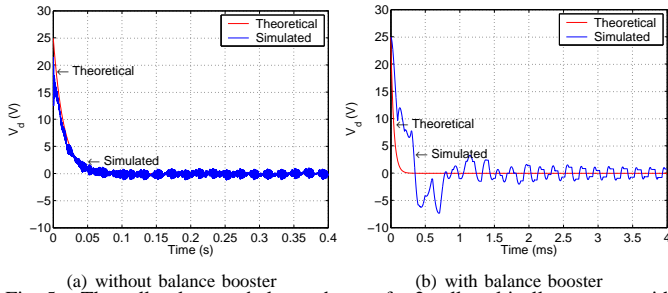


Fig. 5. The cell voltage unbalance decay of a 2-cell multicell converter with $f_r = 50$ Hz, $f_s = 5$ kHz and $m_a = 0.6$.

connected in parallel with the load was tuned to 5 kHz. The values of the balancing circuit parameters are listed in Table I. In these results it can be seen that the cell capacitor voltage balances significantly

faster than for the case without the balance booster circuit connected.

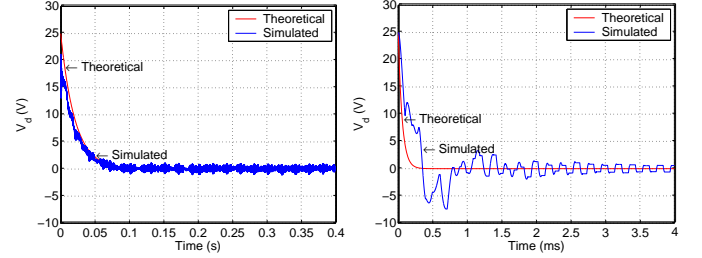


Fig. 6. The cell voltage unbalance decay of a 2-cell multicell converter with $f_r = 50$ Hz, $f_s = 5$ kHz and $m_a = 0.8$.

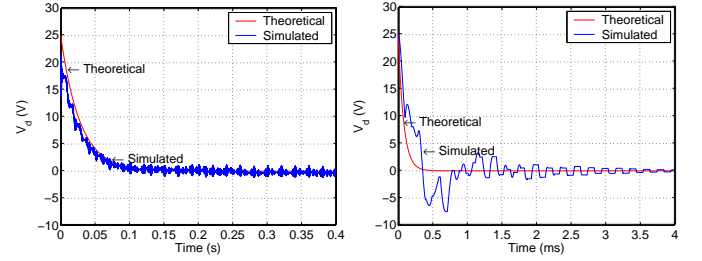


Fig. 7. The cell voltage unbalance decay of a 2-cell multicell converter with $f_r = 50$ Hz, $f_s = 5$ kHz and $m_a = 1.0$.

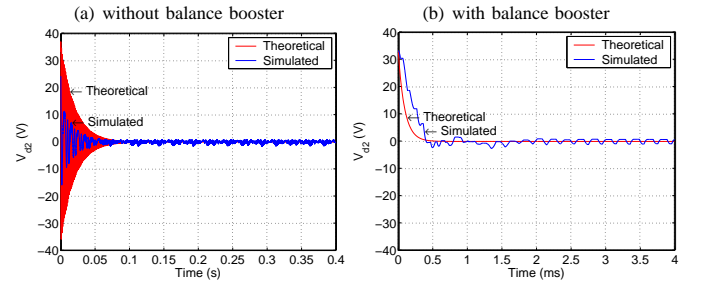
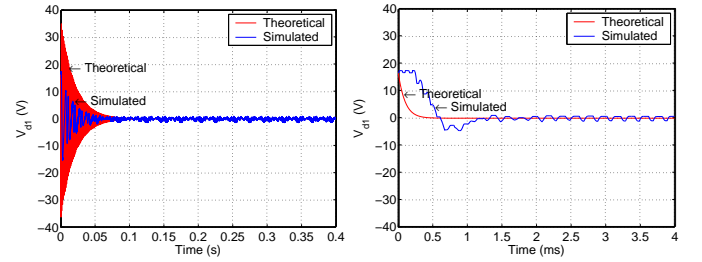


Fig. 8. The cell voltage unbalance decay of a 3-cell multicell converter with $f_r = 50$ Hz, $f_s = 5$ kHz and $m_a = 0.6$.

VI. CONCLUSIONS AND FUTURE WORK

A p -cell multicell converter was modeled and analyzed mathematically. This analysis included that of the self-balancing property of the cell capacitor voltage and the conditions under which this property is valid. Unbalance was also analyzed and conditions shown which lead to voltage unbalance. Future work includes the modeling and analysis of 3-phase multicell converters.

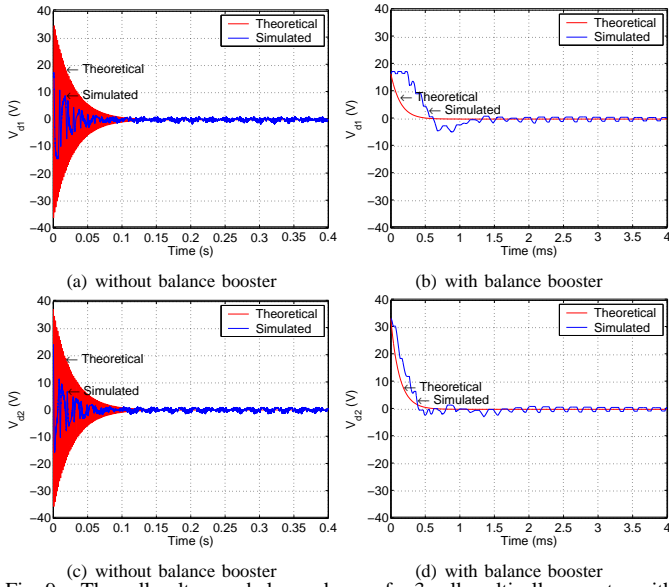


Fig. 9. The cell voltage unbalance decay of a 3-cell multicell converter with $f_r = 50 \text{ Hz}$, $f_s = 5 \text{ kHz}$ and $m_a = 0.8$.

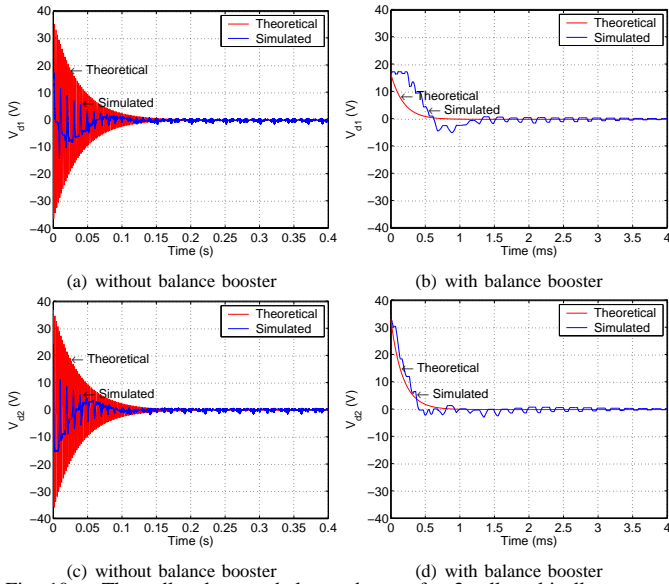


Fig. 10. The cell voltage unbalance decay of a 3-cell multicell converter with $f_r = 50 \text{ Hz}$, $f_s = 5 \text{ kHz}$ and $m_a = 1.0$.

REFERENCES

- [1] O. Tachon, M. Fadel, T.A. Meynard, "Control of series multicell converters by linear state feedback decoupling," *EPE'97 Conference Proceedings*, Trondheim, Norway, September 1997, pp. 1.588-1.593.
- [2] G. Gateau, *Contribution à la Commande des Convertisseurs Statiques Multicellulaires série: Commande Non Linéaire et Commande Floue*, Thèse de L'Institut National Polytechnique de Toulouse, September 1997.
- [3] T.A. Meynard, M. Fadel, N. Aouda, "Modelling of multilevel converters," *IEEE Transactions on Industrial Electronics*, Vol. 44, No. 3, June 1997, pp. 356-364.
- [4] T.A. Meynard, H. Foch, "Multilevel converters and derived topologies for high power conversion," *Conf. Rec. IEEE IECON'95*, Orlando, USA, September 1995, pp. 21-26.
- [5] H. du T. Mouton, *Analysis and synthesis of a 2 MVA series-stacked power-quality conditioner*, Ph.D. Thesis, University of Stellenbosch, December 1999.
- [6] H. du T. Mouton, "Natural balancing of three-level neutral-point-clamped PWM inverters," *IEEE Transactions on Industrial Electronics*, Vol. 49, No. 5, October 2002, pp. 1017-1025.

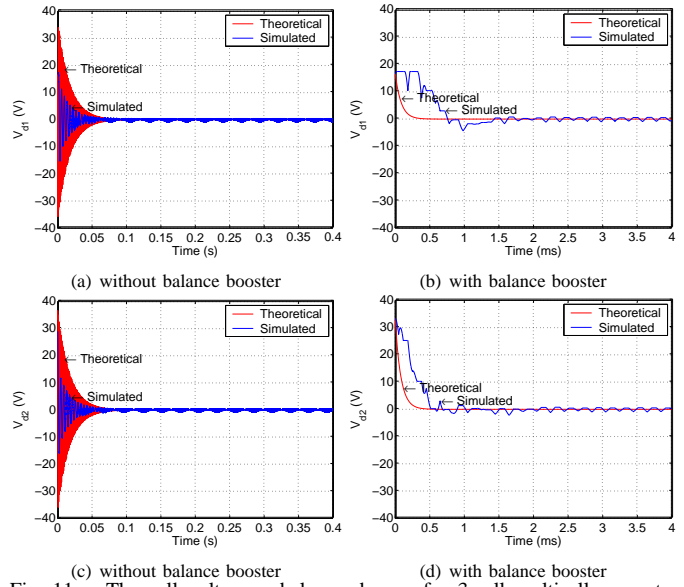


Fig. 11. The cell voltage unbalance decay of a 3-cell multicell converter with a fixed duty-cycle of $D = 0.33$ and $f_s = 5 \text{ kHz}$.

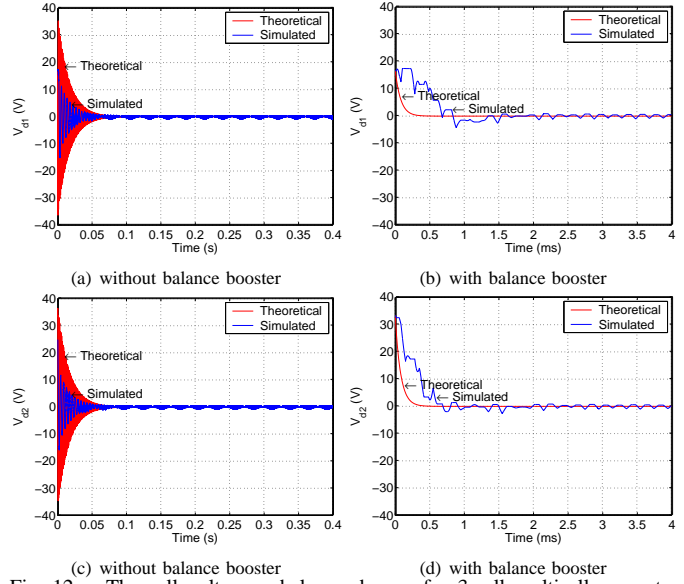


Fig. 12. The cell voltage unbalance decay of a 3-cell multicell converter with a fixed duty-cycle of $D = 0.66$ and $f_s = 5 \text{ kHz}$.

- [7] X. Yuan, H. Stemmler, I. Barbi, "Self-balancing of the clamping-capacitor-voltages in the multilevel capacitor-clamping-inverter under sub-harmonic PWM modulation," *IEEE Trans. on Power Electronics*, Vol. 16, No. 2, March 2001, pp. 256-263.
- [8] S.J. Watkins, L. Zhang, "Modelling and control of a flying capacitor inverter," *EPE'01 Conference Proceedings*, Graz, Austria, August 2001.
- [9] P. Carrere, T.A. Meynard, J.P. Lavieville, "4000 V/300 A eight-level IGBT voltage-source inverter leg," *EPE'95 Conference Proceedings*, Seville, Spain, September 1995.
- [10] R.H. Wilkinson, T.A. Meynard, H. du T. Mouton, "Voltage unbalance in the multicell converter topology," *Conf. Rec. IEEE Africon'02*, George, South Africa, October 2002, pp. 759-764.
- [11] W.R. Bennet, "New results in the calculation of modulation products," *Bell Sytems Technical Journal*, Vol. 12, pp. 228-243, 1933.
- [12] H.S. Black, *Modulation Theory*, D. van Nostrand Company, Inc., Princeton, New Jersey, 1953.
- [13] <http://www.pwr.com>.